



NJC

A Polymeric Bis(di-p-anisylamino)fluorene Hole-Transport Material for Stable n-i-p Perovskite Solar Cells

Journal:	<i>New Journal of Chemistry</i>
Manuscript ID	NJ-ART-08-2020-004157.R1
Article Type:	Paper
Date Submitted by the Author:	03-Jan-2021
Complete List of Authors:	Tremblay, Marie-Hélène; Georgia Institute of Technology, School of Chemistry and Biochemistry Schutt, Kelly; University of Oxford, Physics Zhang, Yadong; Georgia Institute of Technology, School of Chemistry and Biochemistry Barlow, Stephen; Georgia Institute of Technology, School of Chemistry and Biochemistry Snaith, Henry; Oxford, Physics Marder, Seth; Georgia Institute of Technology, School of Chemistry and Biochemistry

SCHOLARONE™
Manuscripts

A Polymeric Bis(di-*p*-anisylamino)fluorene Hole-Transport Material for Stable n-i-p Perovskite Solar Cells

Marie-Hélène Tremblay^a, Kelly Schutt^b, Yadong Zhang^a, Stephen Barlow^a, Henry J. Snaith^b, and Seth R. Marder^{a*}

^a School of Chemistry and Biochemistry, and Center for Organic Photonics and Electronics (COPE), Georgia Institute of Technology GA, Atlanta 30332-0400, United States

^b Clarendon Laboratory, Department of Physics, University of Oxford, Parks Road, Oxford OX1 3PU, United Kingdom

Abstract

A norbornene homopolymer with hole-transporting 2,7-bis(di-*p*-anisylamino)fluorene side chains is compared to the widely used spiro-OMeTAD as a hole-transport material (HTM) in negative-intrinsic-positive (n-i-p) perovskite solar cells (PSCs). PSCs fabricated using p-doped homopolymer achieve a power conversion efficiency of 15.5%, comparable to that of cells incorporating p-doped spiro-OMeTAD as the HTM. However, half-devices made with the polymer exhibit improved light and heat stability in comparison to those incorporating spiro-OMeTAD.

Introduction

Proper choice of hole-transport materials (HTM) is a key factor for efficient and stable lead-halide perovskite solar cells (PSCs). HTMs are necessary to minimize the charge recombination that would occur at direct perovskite:hole-collecting electrode interfaces. Organic molecules, polymers, metallomacrocycles, and inorganic materials can be used as HTMs in PSCs.¹ One of the widely used HTM in high-performance PSCs is spiro-OMeTAD (2,2',7,7'-tetrakis(di-*p*-anisylamino)-9,9'-spirobi[9*H*-fluorene]). Favorable attributes include its ionization energy (IE), which is well-matched with that of the perovskite absorber layer, easy solution processability, good conductivity (when appropriately doped), electrochemical stability, and high glass-transition temperature. Nevertheless, many studies show that the use of spiro-OMeTAD (with additive/dopants) can limit the stability of PSCs.² Crystallization³ and photo-oxidation of spiro-OMeTAD,⁴ as well as diffusion of electrode metal into the HTM layer,⁵ all lead to degradation of the PSC performance. Some of these drawbacks may potentially be addressed by using a polymeric material with similar electronic characteristics to spiro-OMeTAD. Here we report a polymeric HTM, **P1**, designed to have electronic properties similar to spiro-OMeTAD, and its incorporation in n-i-p PSCs (see Fig. 1). The polymeric approach could potentially prevent moisture, dopant, and electrode metal diffusion.

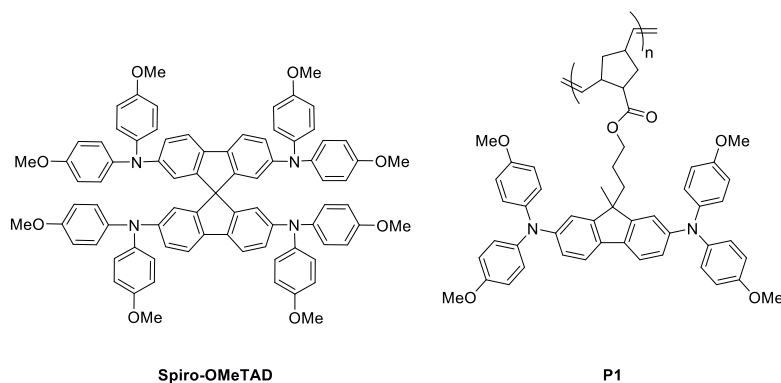


Figure 1. Structure of the widely used spiro-OMeTAD and the HTM, **P1**, reported here.

Results and Discussion

Synthesis

Attaching one polymerizable group to the symmetrical spiro-OMeTAD was anticipated to be synthetically complex. However, the role of the spiro-linkage in spiro-OMeTAD is largely to ensure a high glass-transition temperature, which, in a polymer, can be largely compensated for by an appropriate polymer backbone. Furthermore, the electrochemical and optical properties are primarily determined by the two bis(*p*-anisylamino)fluorene “arms” of the structure.⁶ Thus, we chose to use a bis(*p*-anisylamino)fluorene building block, the 9-position of the fluorene providing an ideal site for introduction of a single polymerizable group, as in some of our previous work on bis(diarylamino)fluorene⁷ and di(carbazolyl)fluorene⁸ side-chain norbornene polymers as hole-transport and host materials for organic light-emitting diodes.

The synthesis of the hole-transporting monomer **M1** was carried out as depicted in Figure 2. First, bis(4-methoxyphenyl)amine and protected-hydroxyl-functionalized 2,7-diiodofluorene were converted to **2** using a Buchwald and Hartwig coupling.^{9, 10} The silyl ether **2** was deprotected to the hydroxyl-functionalized bis(diarylamino)fluorene **3** using tetra-*n*-butylammonium fluoride in tetrahydrofuran. Deprotonation of the alcohol with sodium hydride, followed by an esterification reaction with 5-norbornene-2-carbonyl chloride, gave a mixture of the *endo* and *exo* isomers of monomer **M1**. **P1** was successfully synthesized using the Grubbs 2nd generation initiator (see Fig. 2). The polymer was soluble in a range of organic solvents including THF, chloroform, dichloromethane, and dichlorobenzene. A broadening of the ¹H NMR peaks was observed, consistent with the formation of a polymer. Moreover, an appreciable downfield chemical shift corresponding to the norbornene alkene protons was observed in the ¹H NMR spectrum of the polymer, consistent with ring-opening of the norbornene. Gel permeation chromatography (in CHCl₃) also indicated formation of a polymer and suggested $M_w = 101$ kDa and $\bar{D} = 1.7$.

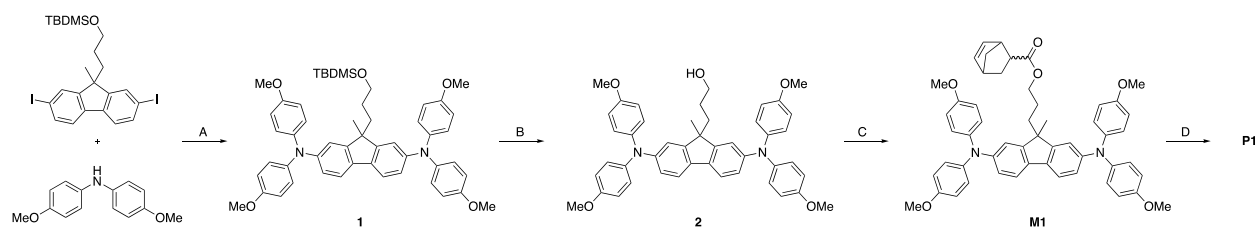


Figure 2. Synthesis of hole-transporting polymer **P1**. (A) Pd(OAc)₂, P^tBu₃, Cs₂CO₃, toluene, (B) ⁿBu₄NF, THF, (C) pyridine, CH₂Cl₂, *endo/exo* 5-norbornene-2-carbonyl chloride, (D) 2nd generation Grubbs initiator (Ru(PCy₃)(=CHPh)LCl₂ (Cy = cyclohexyl; L = 1,3-bis(2,4,6-trimethylphenyl)-2-imidazolidinylidene)).

Characterization of HTM

Electrochemical measurements on the monomer **M1** in CH₂Cl₂/0.1 M Bu₄NPF₆ indicate two successive reversible oxidations at E_{1/2} = +0.57 V and +0.87 V vs internal FeCp*₂⁺⁰ (Cp* = η⁵-C₅Me₅; see Fig. 3A) reference. These values correspond to +0.01 and +0.31 V vs. FeCp₂⁺⁰ and thus the first oxidation allows us to estimate a solid-state IE of 4.8 eV (using the relation give in the footnote of Table 1), which is the same as we obtain for spiro-OMeTAD in the same way. We also compared the optical properties of **P1** and spiro-OMeTAD; as shown in Fig. 3B and Table 1, there are only small differences in the spectra.

Table 1. Physical properties of the synthesized materials and Spiro-OMeTAD.

	λ _{abs} (nm) ^a	λ _{fluo} (nm) ^{a, b}	IE (eV) ^c	EA (eV) ^d	E _g (eV) ^e
M1	307, 366, 381	422	4.8	1.7	3.07
P1	301, 375 ^f	422	-	-	3.06
Spiro-OMeTAD	306, 386	423	4.8	1.8	2.98

^a The spectra were measured in CH₂Cl₂. ^b Measured at 0.1 absorbance at λ_{max}. ^c Estimated using the equation IE (eV) = 4.8 + E_{1/2}⁺⁰ (V), where the E_{1/2}⁺⁰ is relative to FeCp₂⁺⁰. ^d Estimated from EA = IE – E_{opt, gap}. ^e Optical gap calculated using the crossing of normalized absorbance and fluorescence spectra. ^f The differences in maxima reported for **M1** and **P1** are due to minor changes in peak shape; the overall absorption profiles are very similar (see Fig. 3B).

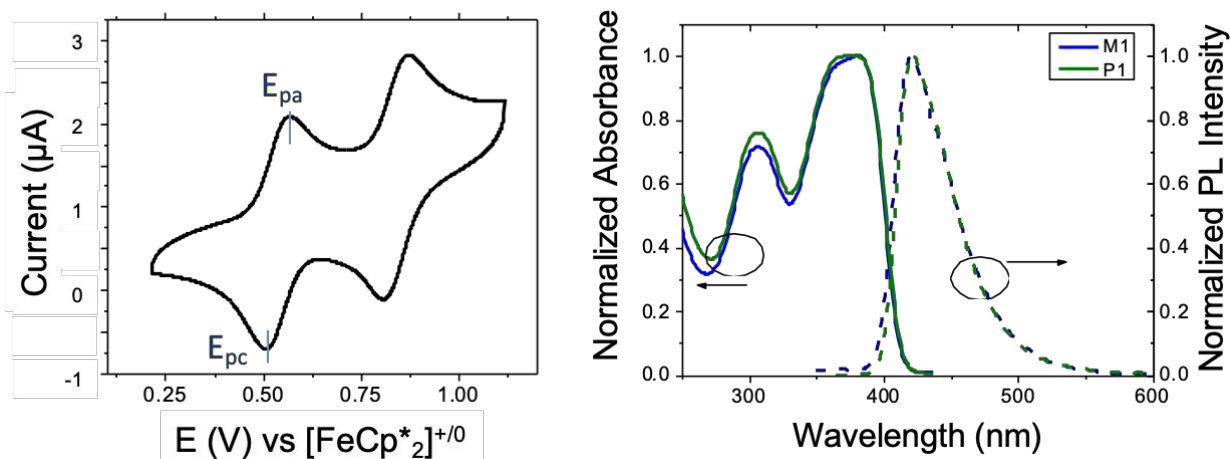


Figure 3. (Left) Cyclic voltammograms of **M1** in CH_2Cl_2 with TBAPF_6 (0.1 M) as an electrolyte with $\text{FeCp}^*_{2^{+}/0}$ ($\text{Cp}^* = \text{C}_5\text{Me}_5$). The half-wave oxidation potential was obtained using the average of the oxidative and reductive peak potentials ($E_{1/2} = (E_{\text{pa}} + E_{\text{pc}})/2$), where E_{pa} and E_{pc} are shown here. (Right) Normalized UV-vis and photoluminescence spectrum of **M1** and **P1** in anhydrous CH_2Cl_2 .

Spiro-OMeTAD generally requires p-doping for satisfactory device performance. The most widely used approach to achieving this p-doping (i.e., partial oxidation to the spiro-OMeTAD radical cation) is to use Li-TFSI (50 mol%) and 4-*tert*-butylpyridine (tBP) (330 mol%) as additives in combination with exposure to air. Other dopants have been tried, including $\text{Mo}(\text{tfd-COCF}_3)_3$, which was used as a dopant for spiro-OMeTAD in n-i-p devices in which no other additive was needed, resulting in higher device stability than when Li-TFSI/tBP doped,^{11, 12} presumably largely due to the absence of the hygroscopic lithium ion, which is thought to promote moisture-induced degradation of the perovskite.¹³ As expected from the similar redox potentials for spiro-OMeTAD and **P1**, optical absorption measurements upon addition of Li-TFSI/tBP or $\text{Mo}(\text{tfd-COCF}_3)_3$ to a solution containing **P1** (see Fig.4) show the growth of new peaks consistent with a bis(diarylamino)fluorene radical cation.

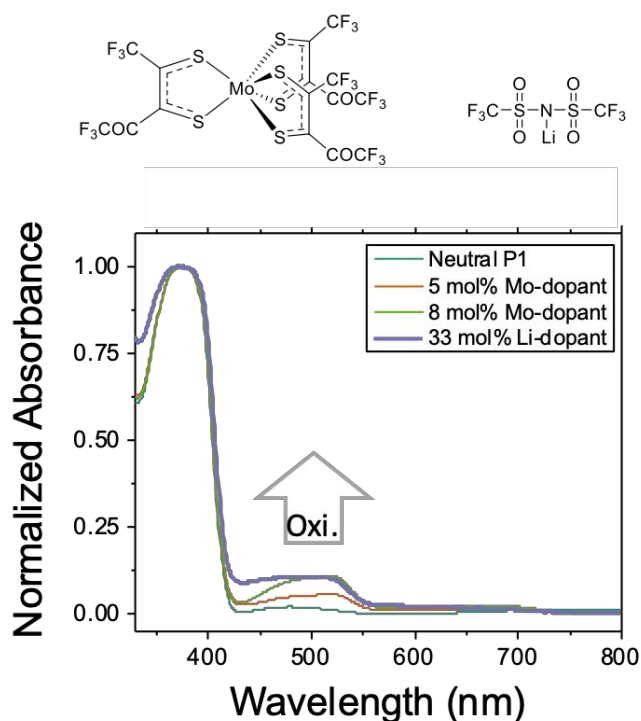


Figure 4. Chemical structure of $\text{Mo}(\text{tfd-COCF}_3)_3$ and Li-TFSI. Doping of **P1** with $\text{Mo}(\text{tfd-COCF}_3)_3$ (taken at $t = 0$ h) and Li-TFSI/tBP (taken after 24 h of air exposure) in CH_2Cl_2 . The weak absorption seen between 600 and 700 nm for the $\text{Mo}(\text{tfd-COCF}_3)_3$ -doped samples is attributable to $\text{Mo}(\text{tfd-COCF}_3)_3^-$.¹⁴

Half-device optical characterization

We aimed to characterize and compare the optical properties of half devices. The Li-TFSI/tBP-doped **P1** and spiro-OMeTAD films spin-coated on top of a $\text{Cs}_{0.05}\text{FA}_{0.95}\text{Pb}(\text{I}_{0.83}\text{Br}_{0.17})_3$ perovskite film on clean glass showed similar PL quenching (PLQE = 0.02 in each case) compared to that of the bare perovskite film (PLQE = 0.28) suggesting comparable losses due to non-radiative recombination at the perovskite/HTM interface, likely related to their similar structures and optical properties.

Deposition of some molecules with Lewis basic substituents on top of the perovskite has been suggested to passivate defects.¹⁵⁻¹⁸ Several studies, including ours, have found ester-containing materials can play a useful role in perovskite growth and/or passivation.¹⁹⁻²² The added ester moieties on the polymer could potentially bind to any undercoordinated lead ions at the surface, effectively screening the charge and reducing recombination. Photoluminescence (PL) lifetime experiments on films of perovskite in contact with doped **P1** or spiro-OMeTAD (see Fig. 5) are consistent with this idea; the former exhibit longer lifetimes associated with bimolecular recombination. Moreover, the PL peak of the **P1**-containing film is blue-shifted compared to the spiro-OMeTAD one, which also suggests that there is passivation of trap states at the interface between the HTM and perovskite layers; removing shallow traps near the band edges effectively blue shifts the photoluminescence.²³

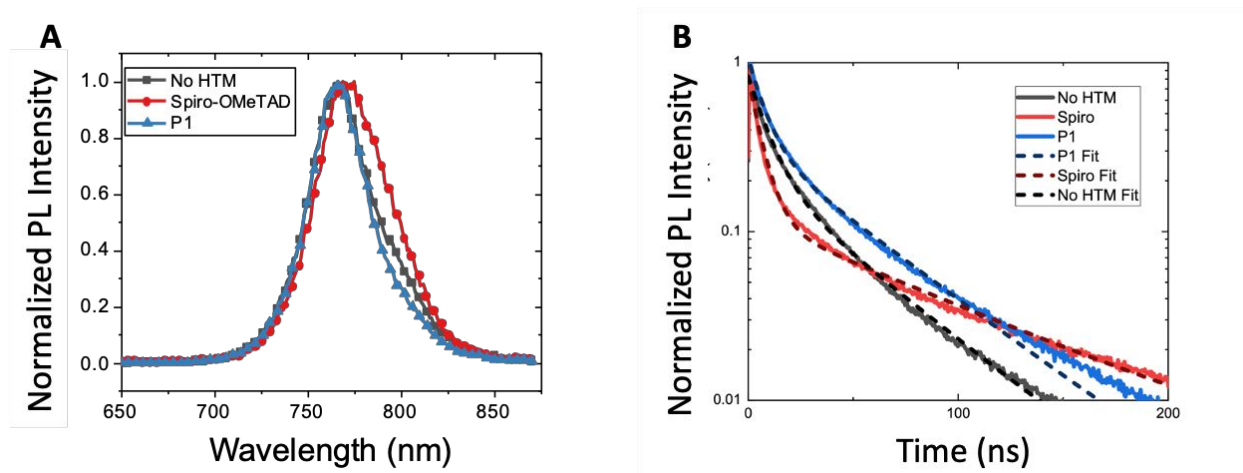


Figure 5. (A) Photoluminescence of glass/perovskite/HTM half devices. The PL maximum for the spiro-OMeTAD sample is slightly red-shifted relative to that of the **P1** and the bare perovskite sample, which may indicate more band-bending due to shallow-trap formation in the spiro-OMeTAD case.^{7,8} (B) Fitting of the time-resolved PL of the glass/perovskite/HTM half devices using a biexponential decay

$$Y = A_1 \exp\left(\frac{-t}{\tau_1}\right) + A_2 \exp\left(\frac{-t}{\tau_2}\right) + y_0$$

where τ_1 is the lifetime for fast, trap-assisted processes (Shockley-Read-Hall recombination), τ_2 is the lifetime for slower bimolecular recombination, and A_1 and A_2 are the relative amplitudes, gave lifetimes $\tau_1 = 7.4$ ns and $\tau_2 = 46.5$ ns for the **P1** sample, while Spiro-OMeTAD sample exhibits a decreased τ_1 value of 5.9 ns and an increased τ_2 lifetime of 80.9 ns. The perovskite on glass reference gave lifetimes $\tau_1 = 8.9$ ns and $\tau_2 = 43.1$ ns.

Half-device stability studies

In addition to possibly passivating the perovskite, it was hypothesized that the polymer could also better protect the perovskite from extrinsic factors (such as moisture or oxygen penetration) compared to the small spiro-OMeTAD molecule.^{24, 25} In order to probe if the polymer **P1** could improve the stability of the solar cells, we fabricated half-cells with the architecture FTO/Cs_{0.05}FA_{0.95}Pb(I_{0.83}Br_{0.17})₃/HTMs (undoped) and heated them in an aging box (conditions: 85 °C, 76 mW cm⁻², 50% relative humidity). We measured the PXRD of the half-cells over time by periodically moving the films to ambient conditions for the time of measurement (see Fig. 6A-B). After 20 h, the bare perovskite film no longer shows the (110) peak of the 3D perovskite at ~14°, while the **P1**- and spiro-OMeTAD-coated films retained 50% and 25% of the peak intensity respectively, clearly showing the advantage of using the polymeric material. We also followed the decomposition of the

perovskite by UV-vis spectroscopy (see Fig. 6C-D). After 48h in the aging box, the spiro-OMeTAD-coated film turned gray and no longer showed a discernable onset of absorption at the perovskite band gap at ~ 775 nm, while for the **P1** containing film, this feature was still observable.

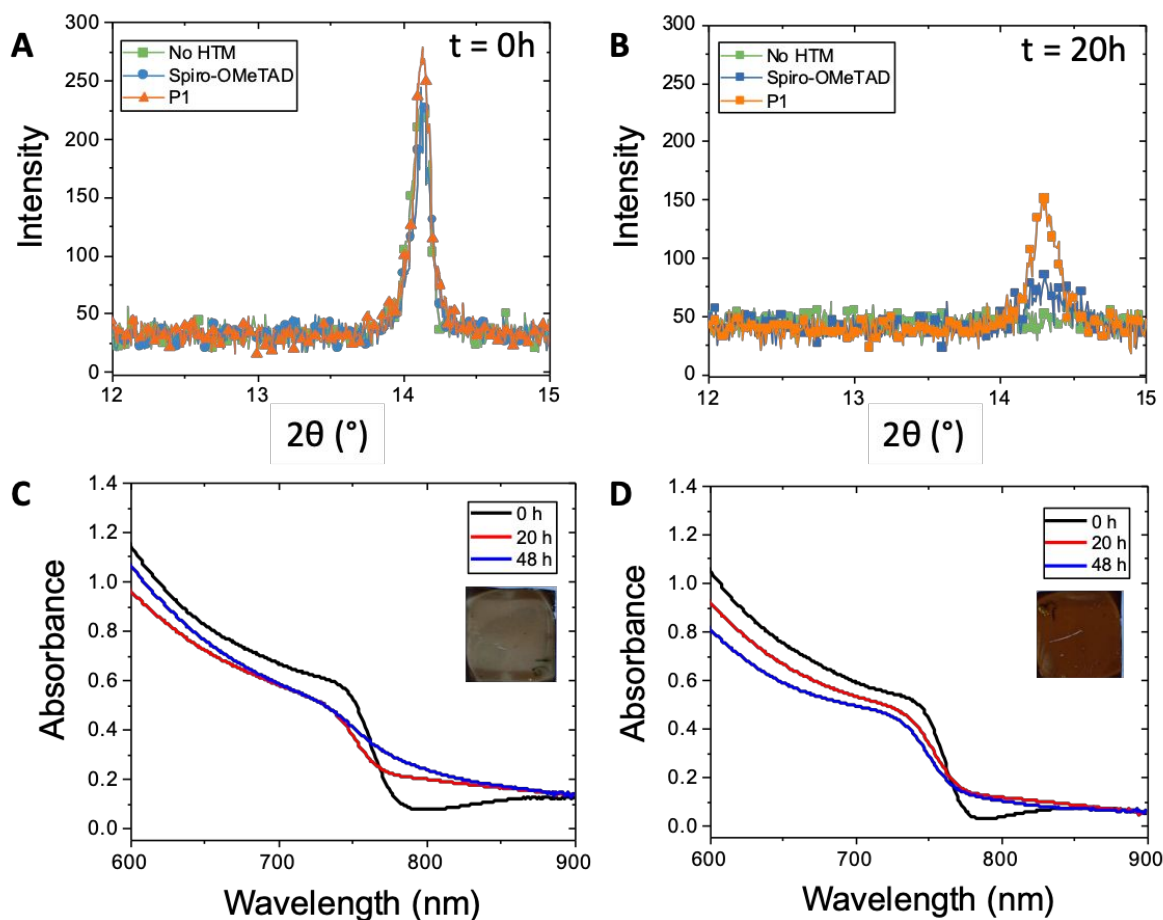


Figure 6. Stability study of the glass/ $\text{Cs}_{0.05}\text{FA}_{0.95}\text{Pb}(\text{I}_{0.83}\text{Br}_{0.17})_3/\text{HTM}$ half devices. PXRD of the films without thermal stress (A) and after 20 h in an aging box (conditions: 85°C , 76 mW cm^{-2} , 50% relative humidity) (B). Absorption spectra after various times under stress in the aging box for samples with (C) spiro-OMeTAD and (D) **P1** as the HTM. Insets: photographs of the films after 48 h in the aging box.

Device fabrication and characterization

We investigated the performance of the new HTM **P1** in n-i-p PSCs using the following architecture; $\text{FTO}/\text{SnO}_2/\text{FA}_{0.85}\text{Cs}_{0.15}\text{Pb}(\text{I}_{0.83}\text{Br}_{0.17})_3/\text{PEA-I}/\text{p-doped HTM}/\text{Ag}$, where FTO = fluorine-doped tin oxide, FA = formamidinium, HTM is spiro-OMeTAD or **P1**, and PEA-I is phenylethylammonium iodide, a known passivating agent.²⁶ The devices using optimally p-doped **P1** (see Supporting Information for optimization of PEA-I, Li-TFSI, **P1** and tBP concentration, Fig. S1-4 and Table S1-4) are reported in Fig. 6 and Table 2. We obtained a champion PCE of 15.5% for Li-TFSI-doped devices, which is similar to that for

the control devices with doped spiro-OMeTAD (16.5%) (see Table S2).²⁷⁻²⁹ The current density–voltage (J–V) characteristics of the best performing devices using Li-TFSI-doped spiro-OMeTAD and **P1** recorded under simulated AM1.5, 1 sun irradiance are presented in Fig. 7. As it can be seen from Table, **P1** and spiro-OMeTAD have similar performance with the averaged performance of **P1** being slightly higher compared to spiro-OMeTAD. The reduced spread in the data also shows improved reproducibility over spiro-OMeTAD, which has previously been shown to form films with poor uniformity.¹⁸ Furthermore, the improved thermal and atmospheric stability of half devices with **P1** suggest that the lifetime power output for devices based on **P1** may be greater than those with spiro-OMeTAD.

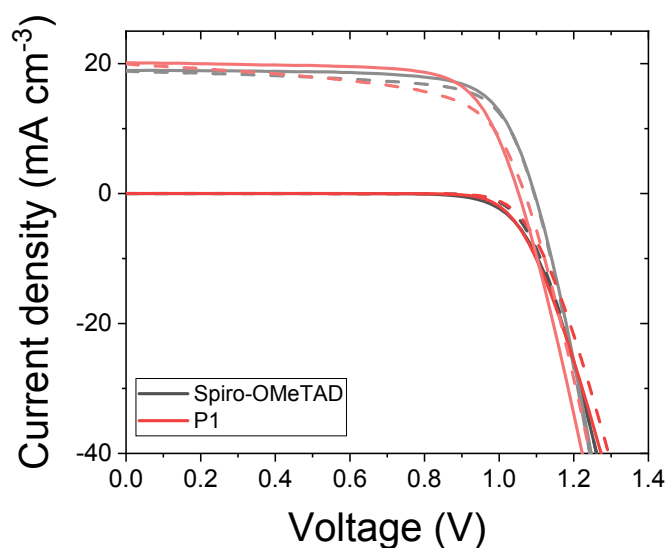


Figure 7. Comparison of the JV curves of the champion cells obtained for Li-TFSI-doped **P1** and spiro-OMeTAD HTMs under 1 sun and in the dark.

Table 2. Basic parameters for the champion n-i-p cell prepared with the two HTMs p-doped using Li-TFSI and tBP.

HTM		PCE (%)	J_{sc} (mA cm ⁻²)	V_{oc} (V)	FF
Spiro-OMeTAD	Average	14 ± 2	18 ± 1	1.06 ± 0.02	0.69 ± 0.03
	Maximum	16.5	19.8	1.10	0.75
P1	Average	14.6 ± 0.9	19.3 ± 0.8	1.05 ± 0.01	0.71 ± 0.02
	Maximum	15.5	20.1	1.06	0.73

Using spiro-OMeTAD ca. 1.5x more material (85 mg mL⁻¹ vs. 55 mg mL⁻¹ for **P1**) is needed to obtain similar photovoltaic performance. The thickness of an optimal **P1** layer was approximately half that of an optimal spiro-OMeTAD layer (~100 nm vs. 200 nm as determined by profilometry). Both doped **P1** and spiro-OMeTAD films have visible “comets”, as is typical for spiro-OMeTAD films. Careful optimization of Li-TFSI and tBP helps to decrease the density of pinholes (see Fig. S6) and to reach optimal device performance. For **P1**, the optimal Li-TFSI dopant concentration is 25 mol%, while that for spiro-OMeTAD is 50 mol%, which in both cases corresponds to oxidation of ¼ of the bis(diarylamino)fluorene units. Moreover, PSCs made with **P1** p-doped using Mo(tfd-COCF₃)₃ (see Fig. S5 and Table S5) were fabricated and achieved similar PCE (14.3 ± 0.9%).

Conclusion

In summary, we have described the use of a polymeric HTM analogue to spiro-OMeTAD in n-i-p PSCs. PCEs using **P1** are as high as 15.5% similar to those obtained using the widely used HTM spiro-OMeTAD. Half-device stability under harsh conditions is also significantly improved when using **P1**, suggesting that it is a promising candidate for single junction and tandem solar cells.

Conflict of interest

There are no conflicts of interest to declare.

Acknowledgement

This work was supported by NSERC (ES. D. Scholarship for MHT), the AFOSR (FA9550-18-1-0499), and the Marshall Aid Commemoration Commission. We thank Khaled Al Kurdi for useful discussions and for the GPC experiment.

References

1. Z. Yu and L. Sun, *Adv. Energy Mater.*, 2015, **5**, 1500213.
2. A. K. Jena, Y. Numata, M. Ikegami and T. Miyasaka, *J. Mater. Chem. A*, 2018, **6**, 2219-2230.
3. X. Zhao, H.-S. Kim, J.-Y. Seo and N.-G. Park, *ACS Appl. Mater. Interfaces*, 2017, **9**, 7148-7153.
4. R. S. Sanchez and E. Mas-Marza, *Solar Energy Mater. Solar Cells*, 2016, **158**, 189-194.
5. K. Domanski, J.-P. Correa-Baena, N. Mine, M. K. Nazeeruddin, A. Abate, M. Saliba, W. Tress, A. Hagfeldt and M. Grätzel, *ACS Nano*, 2016, **10**, 6306-6314.
6. S. Fantacci, F. De Angelis, M. K. Nazeeruddin and M. Grätzel, *J. Phys. Chem. C*, 2011, **115**, 23126-23133.
7. R. D. Hreha, A. Haldi, B. Domercq, S. Barlow, B. Kippelen and S. R. Marder, *Tetrahedron*, 2004, **60**, 7169-7176.
8. J.-Y. Cho, B. Domercq, S. Barlow, K. Y. Saponitsky, J. Li, T. V. Timofeeva, S. C. Jones, L. E. Hayden, A. Kimyonok, C. R. South, M. Weck, B. Kippelen and S. R. Marder, *Organometallics*, 2007, **26**, 4816-4829.

9. D. Baranamo, G. Mann and J. F. Hartwig, *Curr. Org. Chem.*, 1997, **1**, 287-305.
10. B. H. Yang and S. L. Buchwald, *J. Organomet. Chem.*, 1999, **576**, 125-146.
11. A. Pellaroque, N. K. Noel, S. N. Habisreutinger, Y. Zhang, S. Barlow, S. R. Marder and H. J. Snaith, *ACS Energy Lett.*, 2017, **2**, 2044-2050.
12. Z. Li, C. Xiao, Y. Yang, S. P. Harvey, D. H. Kim, J. A. Christians, M. Yang, P. Schulz, S. U. Nanayakkara, C.-S. Jiang, J. M. Luther, J. J. Berry, M. C. Beard, M. M. Al-Jassim and K. Zhu, *Energy Environ. Sci.*, 2017, **10**, 1234-1242.
13. Y. Li, Y. Wang, T. Zhang, S. Yoriya, P. Kumnorkaew, S. Chen, X. Guo and Y. Zhao, *Chem. Commun.*, 2018, **54**, 9809-9812.
14. S. K. Mohapatra, Y. Zhang, B. Sandhu, M. S. Fonari, T. V. Timofeeva, S. R. Marder and S. Barlow, *Polyhedron*, 2016, **116**, 88-95.
15. M. Saliba, S. Orlandi, T. Matsui, S. Aghazada, M. Cavazzini, J.-P. Correa-Baena, P. Gao, R. Scopelliti, E. Mosconi, K.-H. Dahmen, F. De Angelis, A. Abate, A. Hagfeldt, G. Pozzi, M. Graetzel and M. K. Nazeeruddin, *Nat. Energy*, 2016, **1**, 15017.
16. H. Zhang, L. Xue, J. Han, Y. Q. Fu, Y. Shen, Z. Zhang, Y. Li and M. Wang, *J. Mater. Chem. A*, 2016, **4**, 8724-8733.
17. B. Chaudhary, A. Kulkarni, A. K. Jena, M. Ikegami, Y. Udagawa, H. Kunugita, K. Ema and T. Miyasaka, *ChemSusChem*, 2017, **10**, 2473-2479.
18. M. L. Petrus, K. Schutt, M. T. Sirtl, E. M. Hutter, A. C. Closs, J. M. Ball, J. C. Bijleveld, A. Petrozza, T. Bein, T. J. Dingemans, T. J. Savenije, H. Snaith and P. Docampo, *Adv. Energy Mater.*, 2018, **8**, 1801605.
19. D. Bi, C. Yi, J. Luo, J.-D. Décoppet, F. Zhang, Shaik M. Zakeeruddin, X. Li, A. Hagfeldt and M. Grätzel, *Nat. Energy*, 2016, **1**, 16142.
20. M.-H. Tremblay, K. Schutt, Y. Zhang, J. Lim, Y.-H. Lin, J. H. Warby, S. Barlow, H. J. Snaith and S. R. Marder, *Sustain. Energy Fuels*, 2020, **4**, 190-198.
21. F. Wang, A. Shimazaki, F. Yang, K. Kanahashi, K. Matsuki, Y. Miyauchi, T. Takenobu, A. Wakamiya, Y. Murata and K. Matsuda, *J. Phys. Chem. C*, 2017, **121**, 1562-1568.
22. X. Liu, Y. Cheng, C. Liu, T. Zhang, N. Zhang, S. Zhang, J. Chen, Q. Xu, J. Ouyang and H. Gong, *Energy Environ. Sci.*, 2019, **12**, 1622-1633.
23. Y. Shao, Z. Xiao, C. Bi, Y. Yuan and J. Huang, *Nat. Commun.*, 2014, **5**, 5784.
24. P. Zhao, B. J. Kim and H. S. Jung, *Mater. Today Energy*, 2018, **7**, 267-286.
25. A. Rajagopal, K. Yao and A. K. Y. Jen, *Adv. Mater.*, 2018, **30**, 1800455.
26. D. S. Lee, J. S. Yun, J. Kim, A. M. Soufiani, S. Chen, Y. Cho, X. Deng, J. Seidel, S. Lim, S. Huang and A. W. Y. Ho-Baillie, *ACS Energy Lett.*, 2018, **3**, 647-654.
27. The n-type contact was not fully optimized. Metal oxides are notoriously sensitive to ambient conditions for their oxidation state, defect density, and surface chemistry which explains the lower performance compared to fully optimized devices (see references 28 and 29)
28. H. Song, Y. Ma, D. Ko, S. Jo, D. C. Hyun, C. S. Kim, H.-J. Oh, J. Kim, *Appl. Surf. Sci.*, 2020, **512**, 145660
29. Q. Kuang, C. Lao, Z. L. Wang, Z. Xie, L. Zheng, *J. Am. Chem. Soc.* 2007, **129**, 19, 6070-6071